High magnetic field study of $CePd_2Si_2$

I. Sheikin,[1,2,*] A. Gröger,[2] S. Raymond,[1,3] D. Jaccard,[1] D. Aoki,[4] H. Harima,[5] and J. Flouquet[3]
[1]*University of Geneva, DPMC, 24 Quai Ernest-Ansermet, 1211 Geneva 4, Switzerland*
[2]*Grenoble High Magnetic Field Laboratory, MPI-FKF/CNRS, BP166, 38042 Grenoble Cedex 9, France*
[3]*Département de Recherche Fondamentale sur la Matière Condensée, SPSMS, CEA/Grenoble, 17 rue des Martyrs, 38054 Grenoble Cedex 9, France*
[4]*Centre de Recherches sur les Très Basses Températures, CNRS, Boîte Postale 166, 38042 Grenoble, France*
[5]*The Institute of Scientific and Industrial Research, Osaka University, Ibaraki, Osaka 567-0047, Japan*
(Received 14 November 2002; revised manuscript received 23 January 2003; published 25 March 2003)

The de Haas–van Alphen (dHvA) effect in the heavy fermion system $CePd_2Si_2$ was studied by magnetic torque measurements in magnetic fields up to 28 T at low temperature. A clear magnetic torque anomaly observed at $B_m \sim 10$ T applied along the crystallographic *a* axis indicates a metamagnetic transition. The transition also manifests itself by a sharp drop of the magnetoresistance at low temperature. The dHvA oscillations observed above the transition reveal six different frequencies in the basal plane with the corresponding effective masses from $6m_e$ to $23m_e$. Comparison of the angular dependence of the dHvA frequencies with the theoretical band-structure calculations implies that the $4f$ electrons are itinerant rather than localized inside a magnetically ordered state. One frequency is split into two close satellites, which most likely originate from the up and down spin bands, whose effective masses differ by a factor of 2. The spin splitting gives rise to an apparent anomalous field dependence of the effective mass obtained from the experiment.

DOI: 10.1103/PhysRevB.67.094420 PACS number(s): 71.18.+y, 71.27.+a, 75.30.Kz

I. INTRODUCTION

At zero pressure ($P=0$), the tetragonal heavy-fermion material $CePd_2Si_2$ belongs to the class of long-range magnetically ordered Kondo compounds. Below its ordering temperature $T_N \sim 10$ K, antiferromagnetism appears with a sublattice magnetization $m_0 = 0.6\mu_B$ at low temperature ($T/T_N \ll 1$).[1] Low-temperature specific heat measurements reveal a large Sommerfeld coefficient $\gamma \sim 100$ mJ/K^2 mol[2,3] quite similar to that found in other cerium-based Kondo antiferromagnets such as $CeAl_2$ (Ref. 4) or $CeIn_3$.[5]

The appearance of superconductivity in $CePd_2Si_2$ near its quantum critical point ($P_c \sim 27$ kbar), first discovered by Mathur *et al.*,[6] is now well established for pure samples, where the clean limit is achieved, i.e., the electronic mean-free-path l_e is larger than the superconducting coherence length ξ_0.[7–11] The unconventional superconductivity seems to be mediated by magnetic fluctuations. However, a precise determination of the boundary between magnetic, superconducting, and paramagnetic phases is still missing.

An important issue for heavy-fermion systems is the determination of the Fermi surface (FS), since there are debates on the localization of the $4f$ electrons on both sides of P_c (Ref. 12) related to low dimensionality[13] and even the superconducting state.[14] At very low temperature, the FS can be determined from the de Haas–van Alphen (dHvA) effect or other quantum oscillation effects observable in magnetic field (B) sweep experiments. The extrapolation of the FS to zero field becomes difficult when the magnetic field itself modifies the magnetic correlations and thus, by feedback, the electronic structure, i.e. the FS topology, effective masses and even their dependence on the spin orientation. There are many examples of magnetically ordered Kondo systems such as $CeAl_2$,[15] $CeIn_3$,[16] CeB_6,[17] or $CeRh_2Si_2$,[18] where the $4f$ electrons are claimed to be localized since the FS topology is that of the lanthanum-based analogs ($LaAl_2$, $LaIn_3$, LaB_6, or $LaRh_2Si_2$, respectively). In the well-known case of $CeRu_2Si_2$, which is at zero pressure already just on the paramagnetic verge of the quantum critical point ($P_c = -10$ kbar) at low field (i.e., below its metamagnetic crossover field $B_m = 7.2$ T), the $4f$ electrons are itinerant, while above B_m the detected dHvA frequencies correspond to the $LaRu_2Si_2$ case. However, full determination of the FS is far from being achieved since the measured FS areas are far too small to account for the still large contribution of the electronic specific heat γ.[19,20] Theoretical arguments based on the treatment of the Kondo lattice at one dimension[21] or on the continuity in the Andersen lattice as the on-site repulsion U increases[22] have led to the conclusion that the $4f$ electrons must appear as itinerant on both sides of P_c. On the other hand, in magnetically ordered Kondo compounds, the molecular field acting on the $4f$ electrons is often comparable to the electronic bandwidth, which is, in turn, related to the single ion Kondo temperature T_K, and thus to the Néel temperature T_N. A strong shift of the electronic levels from the paramagnetic state can be expected, which leads to an apparent localization of the $4f$ electrons. Furthermore, for the rather high magnetic field ($B \gtrsim 12$ T) required to observe quantum oscillations in $CePd_2Si_2$, the magnetic polarization itself is already strong, as can be concluded from the susceptibility and neutron diffraction measurements at zero and low field.[1] A strong magnetic polarization also leads to the localization of the $4f$ electrons. By contrast, above the quantum critical point, the FS observed for $CeRu_2Si_2$ at low field (i.e., weak magnetic polarization) is that calculated with itinerant $4f$ electrons. The question of the localization of the $4f$ electrons is, therefore, not so straightforward. So far, there are no full calculations taking into account molecular and magnetic field effects.

 ©2003 The American Physical Society

The main aim of this work is to present quantum oscillation data on $CePd_2Si_2$ by comparison to band-structure calculations realized with two hypothesis: localization or itineracy of the $4f$ electrons. We will also focus on the field dependence of the effective mass as well as on the difference between majority and minority spin carriers.

II. EXPERIMENTAL DETAILS

All the high magnetic field measurements reported here have been performed on the same single crystal that had been previously studied in the high pressure experiments.[9] Details of the sample preparation and characterization are given elsewhere.[7] The sample dimensions are $630\times150\times70\ \mu m^3$, with its *a* and *c* axes parallel to its length and width respectively.

The magnetoresistance was measured by a standard ac technique with a lock-in detection. The current of 100 μA at a frequency of 11.7 Hz was applied along the length of the sample, being parallel to its *a* axis. The measurements were performed in a $^3He/^4He$ dilution refrigerator at 100 mK and 4.2 K; the magnetic fields up to 16 T parallel to the sample *a* axis were generated by a superconducting magnet.

The measurements of the magnetic torque were performed at the M6, M9, and M10 Bitter magnets of the Grenoble High Magnetic Field Laboratory. For these measurements, the sample was mounted in a top-loading dilution refrigerator equipped with a system allowing the sample to be rotated *in situ*. In most of the measurements, *c* axis of the sample was parallel to the rotation axis. Since the rotation axis was perpendicular to the field direction, this allowed the magnetic fields up to 23 or 28 T to be tilted in the sample basal plane. Some sweeps were also done up to 18 T applied in the *ac* plane.

A torque technique was used for the quantum oscillation measurements. In this technique, a sample is mounted on a cantilever, which represents also the upper plate of a capacitor. When a magnetic field $\vec{B}$ is applied, the sample experiences a torque $\vec{T}=\vec{M}\times\vec{B}$, where $\vec{M}$ is the magnetization of the sample. The torque acting on the sample bends the cantilever and the capacitance varies. For a small deformation of the cantilever, the capacitance variations can be assumed as proportional to the torque. Thus, the measurements of the capacitance variation provide a measure of torque *T* given by

$$T=M_{\perp}BV, \tag{1}$$

where $M_{\perp}$ is the sample magnetization component perpendicular to the magnetic field and *V* is the sample volume.

For the materials with an anisotropic Fermi surface, the oscillatory part of the magnetization $\tilde{M}$ has a component perpendicular to the magnetic field, which is given by

$$\tilde{M}_{\perp}=\frac{1}{F}\frac{\partial F}{\partial \theta}\tilde{M}_{\parallel}, \tag{2}$$

where $\tilde{M}_{\parallel}$ is a parallel component, *F* is the dHvA frequency, and θ is the orientation of the Fermi surface with respect to the applied filed. In a normal metal, $\tilde{M}_{\parallel}$ would be given by the usual Lifshitz-Kosevich formula. However, there is no general theory for $\tilde{M}_{\parallel}$ in heavy fermion systems. Nonetheless, it is believed that its general form will closely resemble that of normal metals, modified by the strong electron correlations. Model calculations by Wasserman, Springford, and Hewson[23] and by Rasul[24] seem to confirm this assumption.

III. RESULTS AND DISCUSSION

A. Metamagnetic transition and magnetic phase diagram

Few studies of $CePd_2Si_2$ in high magnetic fields exist. Abe *et al.*[25] presented magnetization at 4.2 K with the magnetic field applied along both *a* and *c* crystallographic axes. For both orientations of the magnetic field, the magnetization was found to increase continuously without showing any anomaly up to 28 T. Heuser *et al.*[26] measured the specific heat of a polycrystalline sample at 0, 13, and 28.9 T. At 28.9 T, the antiferromagnetic transition was found to be broadened with both the peak in the specific heat and the transition midpoint suppressed to lower temperatures though the onset did not shift.

Recently, specific heat measurements on $CePd_2Si_2$ in magnetic fields up to 16 T were reported.[3] The measurements were performed on a single crystal much bigger than that we used in this study. The crystal, however, was grown by a different technique and was very similar to that reported in Ref. 1. Compared to our sample, it showed significantly higher residual resistivity ($\rho_0\sim20\ \mu\Omega$ cm instead of $\rho_0=1\ \mu\Omega$ cm here) and lower $T_N=9.3$ K compared to 10.2 K for our crystal. The antiferromagnetic transition was found to shift to lower temperatures when a magnetic field was applied along the crystallographic *a* axis, while a field applied parallel to the tetragonal *c* axis did not affect the transition.[3] It was also found that the low-temperature term of the specific heat, γ_0, shows a maximum around $B=6$ T. Both the suppression of the antiferromagnetic transition temperature and the appearance of a maximum in γ_0 observed in the specific heat measurements[3] are consistent with the results of a recent magnetization study[27] performed on a sample from the same batch as Ref. 3. The differential susceptibility was found to show a rather broad, but still well-defined maximum at about 6 T. The position of the maximum was almost temperature independent up to 8 K. These observations suggest the existence of an additional transition inside the antiferromagnetic state, presumably of the metamagnetic nature.

Here we report convincing evidence of the presence of a metamagnetic transition, although we find it at a higher field than that suggested by the previous study,[3] as will be discussed later. Figure 1(a) shows the field dependence of the magnetic torque for different directions of the magnetic field with respect to the *a* axis in the basal plane. The magnetic torque increases rapidly at low field, then showing a distinct kink [indicated by arrows in Fig. 1(a)] at about 10 T. The anomaly in the magnetic torque found here is quite similar to that observed in UPd_2Al_3 at 18 T,[28] where it is well established to correspond to a metamagnetic transition. For $B\|a$, the kink in the magnetic torque corresponds to a sharp minimum of the magnetoresistance measured at 0.1 K, as shown

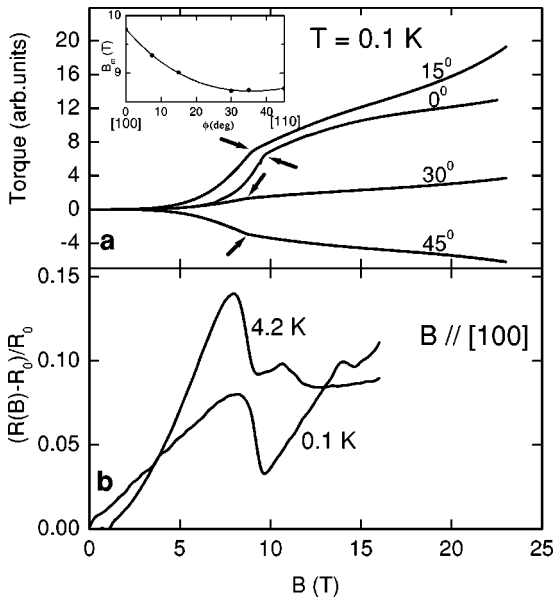

FIG. 1. (a) Field dependence of the magnetic torque for several given orientations of the field in the basal plane. The arrows indicate the anomalies corresponding to the metamagnetic transition. The inset shows angular dependence of the magnetic field at which the anomaly occurs in the basal plane. (b) Normalized magnetoresistance defined here as $\Delta R = R(B) - R_0$ as a function of the magnetic field applied along the crystallographic *a* axis is shown for $T = 100$ mK and 4.2 K. For both temperatures, a sharp drop of the magnetoresistance manifests the metamagnetic transition also seen as an anomaly in magnetic torque (upper panel).

in Fig. 1(b). At 4.2 K, the minimum shifts to a slightly lower field remaining are, however, quite robust. The origin of smaller anomalies at higher field ($\sim$13 T at 0.1 K and $\sim$11 T at 4.2 K) is not clear. They might be related to the reorientation of magnetic domains, since the magnetoresistance was only measured with the magnetic field applied along [100] direction, i.e., away from the easy magnetic axis ([110] direction). The shape of the resistivity curves closely resembles that reported for URu_2Si_2,[29] where a complex three-step metamagnetic transition is found in the field range 35–40 T. We, therefore, argue that a metamagnetic transition occurs in $CePd_2Si_2$ at $B_m \sim 10$ T, when the magnetic field is applied along the crystallographic *a* axis. The field at which the metamagnetic transition occurs has a weak angular dependence when the magnetic field is tilted in the basal plane, as can be seen in the inset of Fig. 1(a). However, when the magnetic field is inclined in the *ac* plane, the metamagnetic transition shifts to higher fields as $1/\cos\theta$, where θ is the angle between the magnetic field and the *a* axis (see Fig. 2). This implies that only fields parallel to the basal plane can trigger the metamagnetic transition, while a field applied along the *c* axis does not produce any effect. This is consistent with staggered magnetic moments aligned in the basal plane, along the [110] direction. In a good agreement, the antiferromagnetic transition moves to lower temperatures for $B \| a$, and does not shift when a field is applied along the *c* axis. The existence of a strong magnetic anisotropy is a common feature of rare-earth-based compounds.

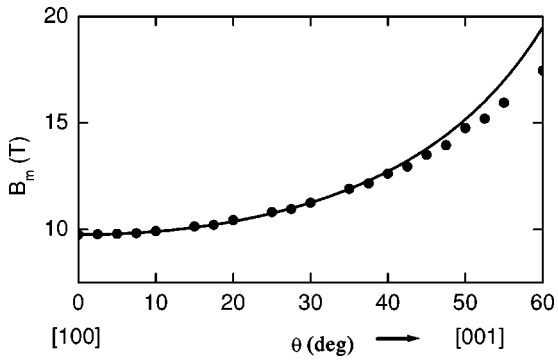

FIG. 2. Angular dependence of the metamagnetic transition field B_m for the field inclined in the *ac* plane. Solid line corresponds to the $B_{m0}/\cos\theta$ dependence with $B_{m0} = 9.8$ T, and θ being the angle from the [100] direction. The small deviation of the experimental points from the calculated curve at high inclination angles is due to the bending of the cantilever.

The above observations combined with some preliminary results of the ac specific heat study of our sample[30] allow us to sketch the magnetic phase diagram of $CePd_2Si_2$. The phase diagram is shown in Fig. 3 for the magnetic field applied along the *a* axis. In agreement with the previously reported results[3] (also shown in Fig. 3), the antiferromagnetic transition temperature T_N decreases with magnetic field. This suggests T_N to be eventually suppressed to zero at higher field as schematically indicated by the gray line in Fig. 3. A metamagnetic transition between two antiferromagnetic phases (denoted as AF1 and AF2 in Fig. 3) is found at $B_m \sim 10$ T at low temperature. The transition shifts to lower field when the temperature increases.

The field dependence of T_N we find here does not match exactly that of Ref. 3. Moreover, the metamagnetic transition field B_m turns out to be higher than the field range, where the low-temperature Sommerfeld coefficient and the differential susceptibility showed a maximum in the previous studies. The discrepancies may be due to differences in the properties

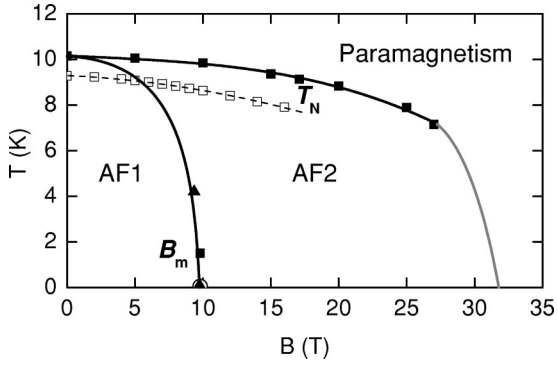

FIG. 3. Magnetic phase diagram of $CePd_2Si_2$ is sketched for $B \| a$ based on the magnetic torque (open circle), magnetoresistance (filled triangles), and AC specific heat (filled squares) measurements. The antiferromagnetic transition temperature T_N as a function of magnetic field from the previous study[3] is also shown as open squares. T_N decreases with magnetic field, suggesting its eventual suppression to zero at higher field as schematically indicated by the gray line. The lines are guide for the eye only.

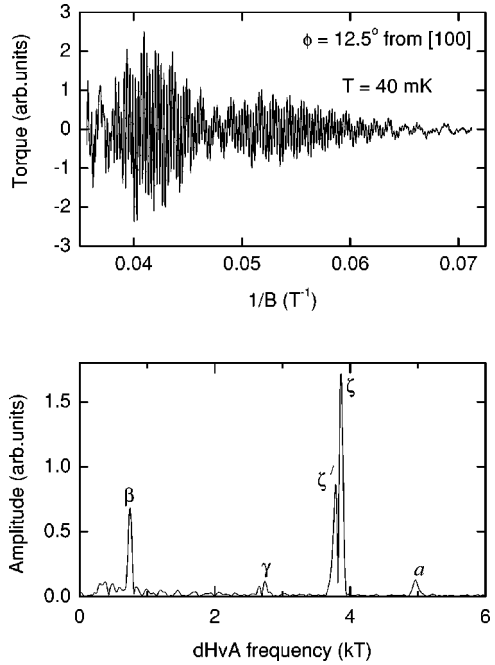

FIG. 4. Typical dHvA oscillatory signal (upper panel) and its Fourier spectrum (lower panel) observed with magnetic field applied at 12.5° from [100] to [110]. The frequencies denoted *a*, β, γ, and ζ are fundamental. Note the splitting of the ζ frequency.

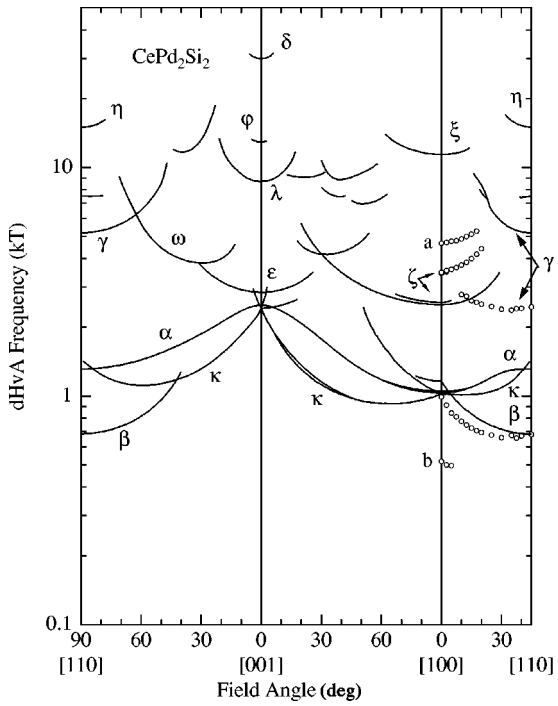

FIG. 5. Angular dependence of the dHvA frequencies obtained from both theoretical band-structure calculation in the itinerant *f* electron model (solid line) and the experiment (open circles). See text for the explanation.

of the samples used for the present and the previous studies. It is already known that only very pure samples ($\rho_0 \lesssim 2\ \mu\Omega$ cm) of $CePd_2Si_2$ show the emergence of superconductivity near the pressure-induced quantum critical point. This is understood in terms of unconventional superconductivity (presumably mediated by antiferromagnetic fluctuations), which is very sensitive to the presence of even nonmagnetic impurities. However, the microscopic origin of the differences in the magnetic properties, i.e., the values and dependence of T_N and B_m, of different quality samples is not clear at present and deserves more systematic study.

B. Angular dependence of the dHvA frequencies

All the observed dHvA oscillations were detected above the metamagnetic transition ($B_m \simeq 10$ T), where the sample is in an intermediate antiferromagnetic state (AF2). Figure 4 shows typical dHvA oscillations and the corresponding FFT (fast Fourier transform) spectrum for the field angle of 12.5° from [100] to [110] direction. The FFT peaks denoted by *a*, ζ, γ, and β are fundamental.

We show in Fig. 5 the angular dependence of the dHvA frequencies; each dHvA frequency F is proportional to the extremal cross-section area of the Fermi surface, $F = S_F \hbar c/2\pi e$. The open circles in Fig. 5 represent the experimental results, while the solid lines show the results of the band-structure calculation described later. Due to the strong magnetic anisotropy, we were able to detect the dHvA signal only for the field directions from [100] to [110], using the present torque technique. Branch β is observed for all orientations of the magnetic field, while the other branches, *a*, ζ, and γ, suddenly disappear at certain field angle, indicating the existence of open orbits.

For the analysis of the effective masses, we assumed the validity of the standard Lifshitz-Kosevich theory, frequently used for other heavy fermion compounds. Theoretical model calculations[23,24] justify such a usage. The cyclotron effective masses were determined from the temperature dependence of the dHvA amplitude. According to the Lifshitz-Kosevich formula, the dHvA amplitude A of a fundamental frequency can be written as follows:

$$A \propto B^{1/2} \left| \frac{\partial^2 S_F}{\partial k^2} \right|^{-1/2} \frac{\alpha m_c^* T/B}{\sinh(\alpha m_c^* T/B)} \exp(-\alpha m_c^* T_D/B), \tag{3}$$

$$\alpha = \frac{2\pi^2 c k_B}{e\hbar} \approx 14.69 \ \text{T/K}, \tag{4}$$

where m_c^* is the cyclotron effective mass and T_D is the Dingle temperature, inversely proportional to the quasiparticle lifetime τ ($T_D = \hbar/2\pi k_B \tau$). Figure 6 shows the so-called mass plot obtained from Eq. (3). From the slope of linear fitting, we determined the cyclotron effective masses, ranging from $6.8m_e$ to $23m_e$ at $B = 24.6$ T for the field angle of 12.5° from [100] to [110] direction.

Although the cyclotron mass is found to vary with field as discussed later, we estimate the Dingle temperature from the field dependence of the dHvA amplitude, where we assume the mass to be constant as a function of field. The Dingle temperature can be obtained from the slope of the plot of $\ln[AB^{1/2}\sinh(\alpha m_c^* T/B)]$ versus $1/B$ according to Eq. (3). For the field angle of 12.5°, the Dingle temperatures are 0.5 K

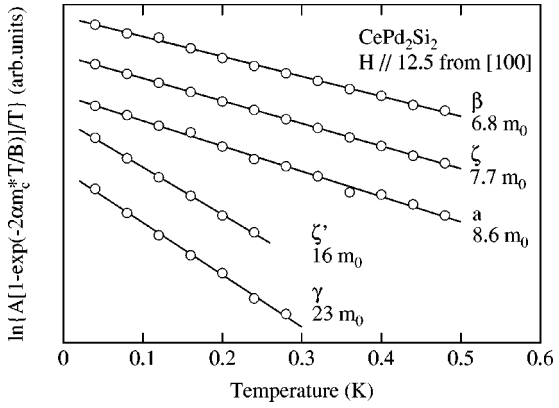

FIG. 6. Mass plot for the same orientation of the magnetic field as in Fig. 4. The slope of the lines allows for the determination of the effective mass, which is found here to vary from $6.8m_e$ to $23m_e$.

and 2.0 K for the branches β and a, respectively. From the following simple relations: $S_F=\pi k_F^2$, $\hbar k_F=m_c^* v_F$, $l=v_F\tau$, we roughly estimate the mean-free-path l as 660 Å for the branch β and 320 Å for the branch a.

As can be seen in Fig. 4, one of the fundamental peaks is split into two satellites ζ and ζ' with frequencies 3.87 and 3.79 kT, respectively. This splitting can be resolved only when analyzing the data up to 28 T, and is not visible over the field range up to 23 T. Furthermore, the difference between the split frequencies depends on the average field of the field range chosen for the analysis. This distinguishes the situation observed for the field angle of 12.5° from the a axis from that for small angles (0 and 2.5°). At small angles, the ζ orbit is also split into two frequencies (denoted ζ_1 and ζ_2 in Table I), but this splitting can be seen in fields up to 23 T and does not depend on the average field of the interval. We believe, therefore, that the splitting we observe at low angles corresponds to that obtained in the band-structure calculation near $B\|[100]$ (see Fig. 5) and is due to a small warping of the corresponding FS. On the other hand, the two close satellites observed at 12.5° most likely originate from the spin splitting of the Fermi surface into the up and down spin bands. For a spin splitting, two sheets of the Fermi surface with opposite orientation of the spins usually have similar shapes and topologies, and thus close values of the effective mass. In our case, however, the effective mass corresponding to the ζ' peak, $16m_e$, is more than two times higher than that of the other satellite (see Fig. 6). This is especially surprising as the difference between the split frequencies is very small ($\Delta F/F\simeq 0.02$) implying that the two corresponding Fermi surfaces have almost the same size. A similar unusual situation has been recently observed in $PrPb_3$,[31] where the effective masses of up and down spin oscillations were found to be very different, up to a factor of 2, although the frequencies were also very close to each other. This remarkable difference, while not easy to understand, might be related to the puzzling situation in some other f electron compounds, e.g., CeB_6,[32,33] where the oscillations from only one spin state were observed. Indeed, this would be the case if the other spin channel had too large effective mass to be observed.

TABLE I. Experimental and calculated dHvA frequencies and effective masses for three orientations of the magnetic field in the basal plane. Branch assignments refer to Fig. 5.

Branch	Experiment		Calculation	
	F (kT)	m^*/m_e	F (kT)	m_b/m_e
		$B\|[100]$		
b	0.52	9.8		
κ			1.02	3.7
α			1.03	0.77
β	0.99	10.2	1.16	1.2
ζ_1	3.44	11.7	2.51	2.0
ζ_2	3.48	6.1	2.57	2.0
a	4.66	9.4		
c	6.11	19.1		
ξ			11.4	5.5
		$B\|7.5°$ from [100] to [110]		
κ			0.93	0.84
β	0.81	7.3	1.01	3.5
α			1.05	0.80
ζ	3.65	7.9	2.57	2.1
a	4.78	10.1		
ξ			11.6	5.9
		$B\|12.5°$ from [100] to [110]		
β	0.75	6.8	0.86	0.77
κ			1.01	3.4
α			1.08	0.86
γ	2.72	23.0		
ζ	3.87	7.7	2.63	2.1
a	4.96	8.6		
ξ			12.0	6.8

C. Theoretical band structure calculation

For $CePd_2Si_2$ and $LaPd_2Si_2$, the band-structure calculations were carried out by using a full potential linearized augmented plane wave (FLAPW) method with the local density approximation (LDA) for the exchange correlation potential. For the LDA, the formula proposed by Gunnarsson and Lundqvist[34] was used. For the band-structure calculation, we used the program codes; TSPACE (Ref. 35) and KANSAI-99. The scalar relativistic effects are taken into account for all electrons and the spin-orbit interactions are included self-consistently for all valence electrons as in a second variational procedure.

The space group of $CePd_2Si_2$ is I4/mmm ($\#139 D_{4h}^{17}$). The lattice parameters used for the calculation are $a=4.2231$ Å and $c=9.8962$ Å, and $z=0.3800$ for $4e$ positions of Si atoms.[36] The same lattice parameters are used for $LaPd_2Si_2$, in which the localized picture is expected. Muffin-tin (MT) radii are set as $0.4041a$ for Ce(La), $0.2790a$ for Pd, and $0.2670a$ for Si. Core electrons [Xe-core minus $5s^25p^6$ for Ce(La), Kr-core minus $4p^6$ for Pd, and Ne-core for Si] are calculated inside the MT spheres in each self-consistent step. $5s^25p^6$ electrons on Ce(La) and $4p^6$ on Pd are calculated as valence electrons by using the second energy window.

The linearized augmented plane wave (LAPW) basis functions were truncated at $|\boldsymbol{k}+\boldsymbol{G}_i|<4.85\times 2\pi/a$, corre-

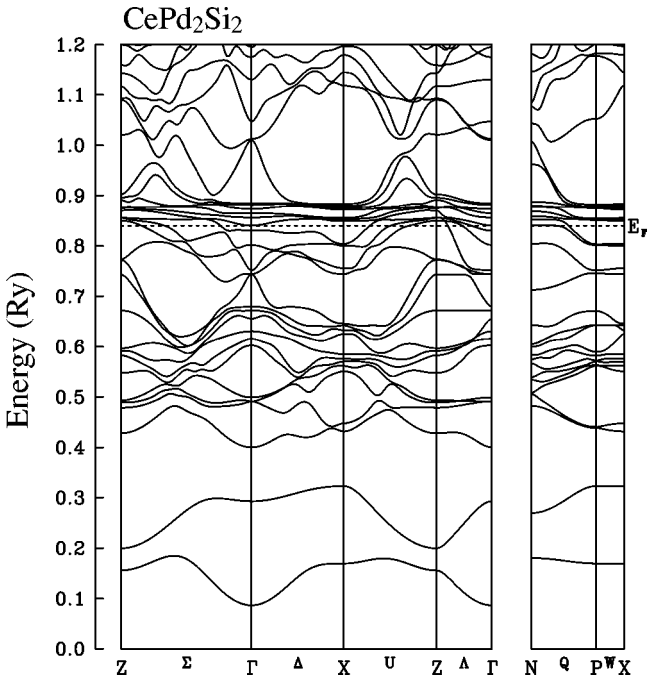

FIG. 7. Calculated band structure along the symmetry axis for $CePd_2Si_2$. The Fermi level is denoted by E_F.

sponding to 567 LAPW functions at the Γ point. The 369 sampling *k* points, which are uniformly distributed in the irreducible 1/16th of the Brillouin zone (divided by 16, 16, and 8), are used both for the potential convergence and for the final band structure. The calculated band structure and the density of states are shown in Figs. 7 and 8, respectively.

D. Comparison to the band structure calculation

In this section, we will compare the experimental results with the results of the band-structure calculation. The solid lines in Fig. 5 represent the calculated angular dependence of the dHvA frequencies based on the $4f$-itinerant band model in the paramagnetic state. Experimental and calculated frequencies and effective masses are also shown in Table I for three orientations of the magnetic field, for which measurements were performed at different temperatures. According to the neutron scattering experiment,[1] the magnetic propagation vector in $CePd_2Si_2$ is $k=[1/2, 1/2, 0]$ and the magnetic moment is oriented along the $[110]$ direction in the antiferromagnetic state. Therefore, compared to the paramagnetic Brillouin zone, the corresponding magnetic one shrinks in size and its volume becomes half of the volume in the paramagnetic state. The dashed line in Fig. 9 shows schematically the magnetic Brillouin zone in the antiferromagnetic state. The real Fermi surfaces also shrink into smaller ones, although relatively small Fermi surfaces situated around the Γ point can be the same as the original ones. Furthermore, if the antiferromagnetic gap energy is small enough compared to the distance between the Landau levels, $\hbar\omega_c$, a magnetic breakdown can occur and the original Fermi surface in the paramagnetic state can be observed even in the antiferromagnetic one. In such a case, the observed dHvA amplitude is smaller than that in the paramagnetic state, because the cyclotron motion is scattered by the magnetic breakdown on the antiferromagnetic gap.

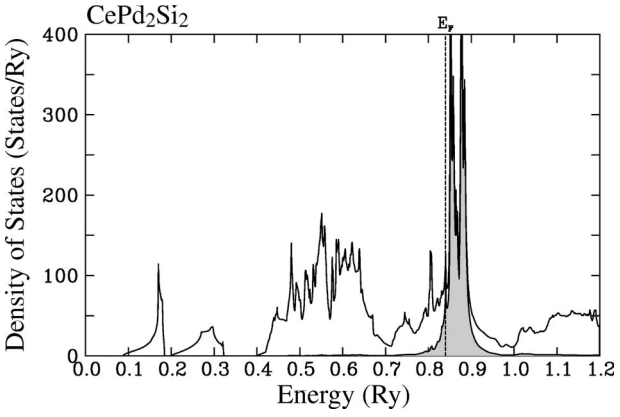

FIG. 8. Calculated density of states for $CePd_2Si_2$. The Fermi level is denoted by E_F. The *f* components of Ce are indicated in gray.

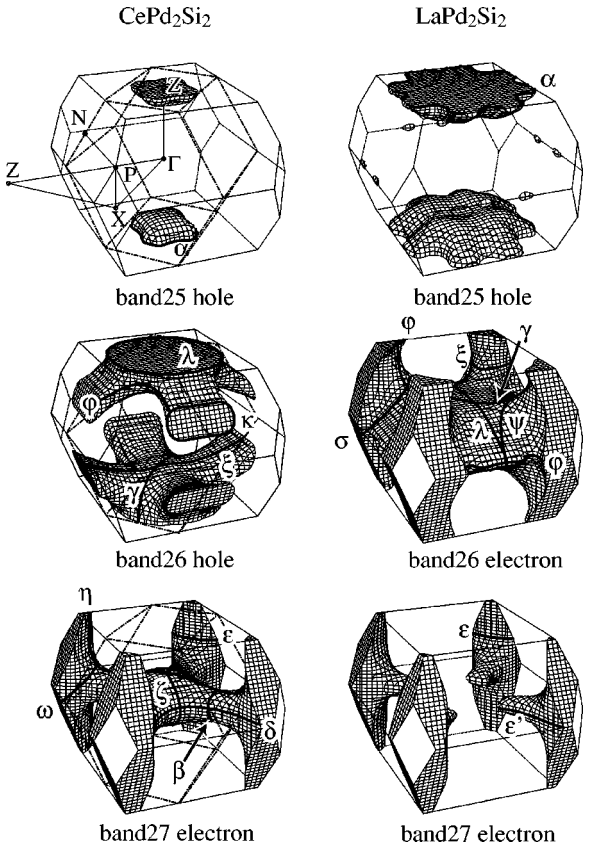

FIG. 9. Calculated Fermi surfaces of $CePd_2Si_2$ and $LaPd_2Si_2$. The calculations were made for a paramagnetic ground state. For $CePd_2Si_2$ in the antiferromagnetic ground state, the modified Brillouin zone (shown by dash-dotted line) is about two times smaller than the paramagnetic one. Also shown the orbits (denoted by Greek letters) that give rise to the corresponding dHvA frequencies shown in Figs. 5 and 10.

As can be seen in Fig. 5, the experimentally observed β branch agrees well with that of the calculations. This branch

corresponds to the arm-shaped Fermi surfaces stretching along the [110] direction, as shown in Fig. 9. Because of the small size of this sheet of the Fermi surface and its position in the Brillouin zone, branch β in the antiferromagnetic state is most likely to be the same as that in the paramagnetic one.

Branch ζ of the experiment is shifted up from the theoretical one, while branch γ of the experiment is shifted down from the theoretical one. This might be attributed to the small shift of the Fermi energy, because branches γ and ζ originate from band 26-hole and band 27-electron Fermi surface, respectively.

For branch *a*, there seems to be no corresponding theoretical branch in Fig. 5. This might be due to the small size of the magnetic Brillouin zone. Although the dHvA frequency of branch *a* is smaller than the allowed maximum frequency of 14 kT in the magnetic Brillouin zone, the Fermi surface located at the zone boundary may be modified by the band folding. Therefore, the *a* branch might originate from branch ξ in the calculation, which corresponds to the multiple-connected Fermi surface, as shown in Fig. 9.

In the experiment branches α and κ were not observed. This is most likely due to the unfavorable curvature factor from the shape of Fermi surface, i.e., $\partial^2 S_F/\partial k^2$ is small for these branches [Eq. (3)].

Next let us consider the cyclotron effective masses. The ratio of the cyclotron mass to the band mass, m_c^*/m_b, is 8.5, 5.9, and 3.05 for branches β, ζ, and ζ', respectively, when the magnetic field is applied along [100] direction (see Table I). On the other hand, for the same orientation of the magnetic field, the ratio of the experimental specific heat coefficient to the calculated one, γ/γ_b, is 17, where the value of γ is equal to 110 mJ/K^2 mol at 15 T [3] and the value of γ_b is equal to 6.2 mJ/K^2 mol. In general, since the many-body effect cannot be fully taken into account in the band calculation, the band mass is smaller than the experimental one. Furthermore, m_c^*/m_b should be equal to γ/γ_b, because both values indicate the same mass enhancement. The discrepancy of the present mass enhancement is likely to indicate that some parts of the Fermi surface corresponding to heavier masses remain unobserved in the present study. Most probably, we have observed only one spin state for most of the bands, while the other spin state corresponding to a larger effective mass and having very close frequency remain hidden. The big difference between the effective masses of branches ζ and ζ' supports this assumption.

E. Itinerant versus localized electrons

We show in Fig. 10 the calculated angular dependence of the dHvA frequencies in $LaPd_2Si_2$. The corresponding Fermi surfaces are also shown in Fig. 9. As La does not contain *f* electrons, these Fermi surfaces correspond to the theoretical ones that are based on the localized *f* electron model in $CePd_2Si_2$, where *f* electrons do not contribute to the Fermi surface. Since the number of electrons that contribute to the band in $LaPd_2Si_2$ is smaller than that in $CePd_2Si_2$, the volume of electron (hole) Fermi surface in $LaPd_2Si_2$ is smaller (larger) than that in $CePd_2Si_2$. For example, the hole band no. 25 Fermi surface of $LaPd_2Si_2$ is larger than that of

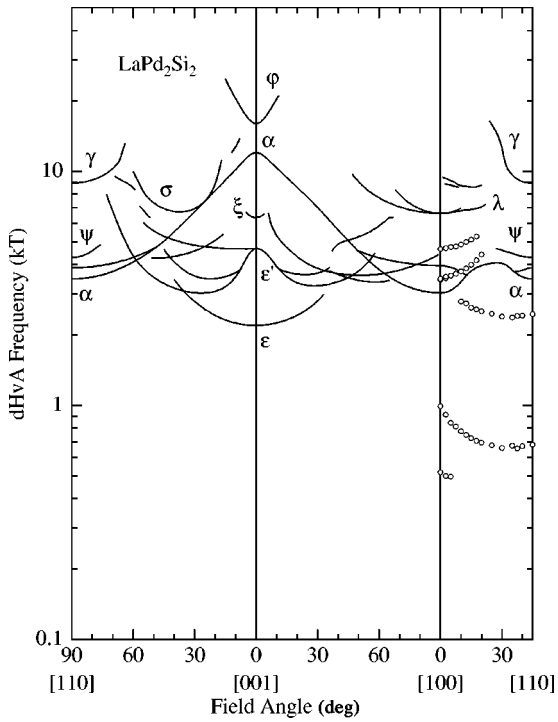

FIG. 10. Angular dependence of the dHvA frequencies obtained from the theoretical band-structure calculation for $LaPd_2Si_2$. The open circles (same as in Fig. 5) represent the experimental results.

$CePd_2Si_2$, while the electron band no. 27 Fermi surface of $CePd_2Si_2$, which is modified from four cylindrical Fermi surfaces of $LaPd_2Si_2$ at the band no. 27, is connected at the Γ point. Comparing the theoretical angular dependence of the dHvA frequencies in $LaPd_2Si_2$ with the experimental one observed in $CePd_2Si_2$, there is no dHvA branch in $LaPd_2Si_2$ corresponding to β branch of the experiment. Furthermore, the existence of the branch ζ in the experiment cannot be explained by the calculation in $LaPd_2Si_2$. Therefore, the experimental results on $CePd_2Si_2$ are not consistent with the $4f$-localized band model. This leads to the conclusion that the *f* electrons of $CePd_2Si_2$ appear to be itinerant rather than localized even in high magnetic field. An open possibility is a partial localization of the *f* electrons, i.e., the situation where a certain fraction of the *f* electrons does not contribute to the FS volume. Such a situation is realized, for example, in CeB_6 where the FS volume obtained from the experiment is only 10% larger than that of LaB_6.[33] This observation led to the conclusion that about 0.1 *f* electrons contribute to the FS volume and therefore can be considered as itinerant, the other ~ 0.9 $4f$ electrons are thus localized.[37] The actual situation in $CePd_2Si_2$ will be clearer when more dHvA frequencies have been detected for different orientations.

F. Field dependence of the effective mass

To study the field dependence of the effective mass, we have performed field sweeps at different temperatures in the range from 30 to 480 mK and up to 23 T applied along the *a* axis and at 7.5° from it, and up to 28 T applied at 12.5° from the *a* axis. The cyclotron masses were determined by fitting

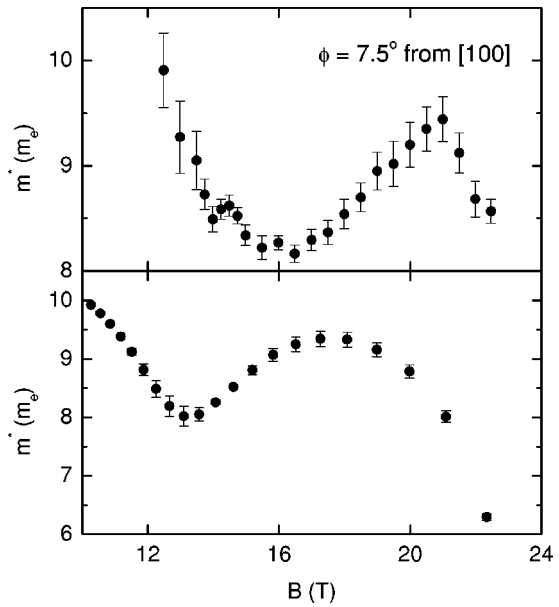

FIG. 11. Field dependence of the cyclotron effective mass for B applied at 7.5° from [100] to [110] obtained from the experiment (upper panel) and from the simulations (lower panel), as described in the text.

the observed temperature dependences of the oscillation amplitude to the Lifshitz-Kosevich form [Eq. (3)]. The effective mass associated with the 3.6 kT orbit that gives the strongest signal has been calculated over 1 T field intervals centered around B_{mean}, the average magnetic field of the intervals. B_{mean} was shifted from 12 to 23 (28) T in steps of 0.5 T.

For all three orientations of the magnetic field, we found an anomalous field dependence of the effective mass, which does not agree with the existing theoretical models. The result obtained for the magnetic field tilted by 7.5° from the *a* axis is shown in the upper panel of Fig. 11. A gradual decrease of the effective mass is clearly observed from $10m_e$ at 12.5 T to $8.1m_e$ at 16 T. Above 16 T, the effective mass increases with magnetic field up to 21 T, where it passes through a broad yet well pronounced maximum. Such a peculiar behavior of the effective mass has been already observed in another heavy fermion compound $CeRu_2Si_2$.[38] In that case, such a behavior of the effective mass was due to the existence of two close frequencies that could not be resolved over small field intervals. This also accounts for our data obtained with magnetic field applied along the crystallographic *a* axis; at this orientation, there are two close fundamental frequencies originating from different Fermi surfaces. However, for the magnetic field applied at 7.5° from the *a* axis, the observed behavior is rather due to the spin splitting of the fundamental frequency, as discussed above. The effective masses of the up and down spin bands are considerably different and seem to be field dependent.

In order to get further, quantitative insight into the nature of the anomalous field dependence of the effective mass, we have performed a wave-form analysis similar to that used by Takashita *et al.*[39] for the case of $CeRu_2Si_2$. We have supposed the existence of two close frequencies originating from the up and down spin states with field-dependent effective masses, which differ from each other. In this case, the dHvA oscillation of a fundamental frequency is given by:

$$D(B,T)=A_{\uparrow}(B,T)\sin\left(\frac{2\pi F_{\uparrow}}{B}-\frac{\pi m^*_{\uparrow}(B)g}{2}+\phi_{\uparrow}\right)+A_{\downarrow}(B,T)\sin\left(\frac{2\pi F_{\downarrow}}{B}+\frac{\pi m^*_{\downarrow}(B)g}{2}+\phi_{\downarrow}\right). \tag{5}$$

Here $A_{\uparrow}$ and $A_{\downarrow}$ denote the amplitude of the oscillations from the up and down spin electrons, respectively. For each direction of the spin, the amplitude is given by Eq. (3), where the Dingle temperature is now different for different orientations of the spin, and the cyclotron effective mass depends both on magnetic field and orientation of the spin. The second term in the oscillation phase arises from the so-called spin-splitting factor $\cos(\pi m^* g/2)$, and the last term is the field-independent phase.

To compare our experimental results with the theoretical model given by Eq. (5), we first extracted only the oscillations within a narrow frequency window around 3600 T from all the data obtained with the magnetic field applied at 7.5° from the *a* axis. We then generated simulated oscillations according to Eq. (5) trying to reproduce the extracted experimental data. We assumed the effective mass ratio $m^*_{\uparrow}/m^*_{\downarrow}=0.48$ to be the same as for 12.5°. Both effective masses were supposed to follow the same field dependence as the low-temperature Sommerfeld coefficient.[3] The latter was extrapolated to higher fields, using the formula proposed by Wasserman *et al.*[23] for the field dependence of the effective mass:

$$m^*(B)=m_b\left[1+\frac{2Dn_f}{Nk_BT_K}\left(1+\frac{Jg\mu_BB}{k_BT_K}\right)^{-2}\right]. \tag{6}$$

In this expression m_b is the band mass, $2D$ is the unrenormalized conduction band width, n_f is the mean occupation number of the f level, g is the electron g factor, μ_B is the free electron Bohr magneton, T_K is the Kondo temperature, and $N=2J+1$ is the f level degeneracy. The field dependence of the low-temperature linear term of the specific heat from Ref. 3 and those of the effective mass of up and down spins used for the simulation are shown in Fig. 12.

Following the above procedure, we have succeeded in obtaining a good simulation of the experimental data for all temperatures. We then calculated the field dependence of the effective mass for the simulated oscillations, using the same procedure as for the original data. The result is shown in the lower panel of Fig. 11. One can see that the peculiar form of $m^*(B)$ obtained from the experiment is qualitatively reproduced by simulations based on the model described above.

IV. CONCLUSIONS

In summary, we performed magnetic torque measurements to study the de Haas–van Alphen effect in the heavy fermion system $CePd_2Si_2$. A distinct anomaly observed in the field dependence of the torque at about 10 T for $B\|a$

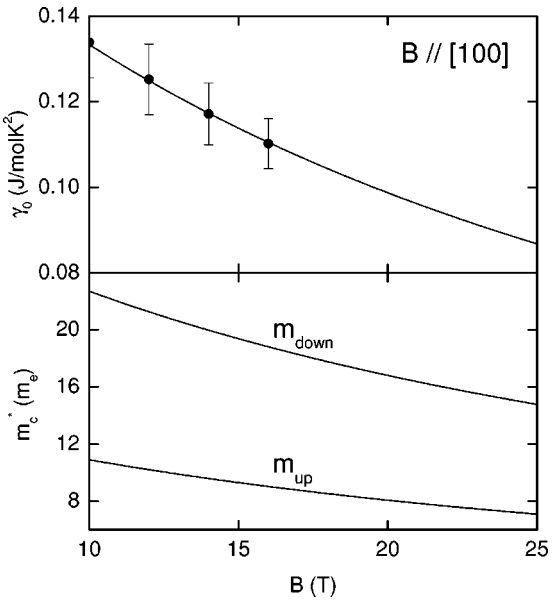

FIG. 12. Upper panel: field dependence of the low-temperature linear term of the specific heat from Ref. 3. The line is a fit by Eq. (6) corresponding to the theoretical field dependence of the effective mass from Ref. 23. Lower panel: field dependence of the effective mass of the up and down spin bands used for the simulation of the oscillatory signal. See text for the explanation.

manifests a transition between two magnetic states. The transition is also seen in the magnetoresistance measurements, where a sudden drop of the resistivity was observed at the same field, $B_m \sim 10$ T at 100 mK. The transition moves to a slightly lower field at $T=4.2$ K implying a rather weak temperature dependence of B_m at low temperature. Based on the above data and those of the preliminary study of the AC specific heat, we have sketched the magnetic phase diagram of this compound for $B \| a$. The phase diagram contains both the antiferromagnetic and metamagnetic transition lines. The value of the magnetic field B_m at which the metamagnetic transition occurs is found to have a weak angular dependence when the magnetic field is tilted in the basal plane. On the other hand, when the magnetic field is inclined in the ac plane, B_m increases as $1/\cos\theta$, where θ is the angle from the basal plane. Thus, only a field component parallel to the basal plane can drive the transition.

Above the metamagnetic transition, in the intermediate AF state, six different dHvA frequencies were detected when the magnetic field is applied in the basal plane. The corresponding effective masses range from $6m_e$ to $23m_e$, which is consistent with a moderate value of the linear specific heat coefficient reported for this compound. The experimentally observed angular dependence of the dHvA frequencies was compared with the theoretical band-structure calculations performed for the paramagnetic state. Taking into account the modification of the Brillouin zone in the AF state and the corresponding change of the Fermi surfaces, the observed angular dependence of the dHvA frequencies favors the results of the band-structure calculations performed for itinerant f electrons. On the other hand, it is difficult to reconcile the experimental results with those of the band-structure calculations for $LaPd_2Si_2$, which would correspond to the localized f electrons. Therefore, the f electrons seem to remain itinerant even above B_m, which is very unusual for Ce-based heavy fermion compounds. It is also possible, however, that a certain fraction of the $4f$ electrons are localized and do not contribute to the FS. To clarify the situation, further measurements at higher, probably pulsed, fields are required to detect more dHvA frequencies.

Let us stress that in $CePd_2Si_2$, the Fermi surface does not present a low-dimensional character in contrast to the case of the new 115 cerium series: $CeRhIn_5$, $CeIrIn_5$, or $CeCoIn_5$.[41–45] It was previously suggested that the low exponent ($n \sim 1.2$) found in the temperature dependence of resistivity, $\rho=\rho_0+AT^n$, of $CePd_2Si_2$ close to P_c, is due to the low dimensionality D of the magnetic correlations.[6] From the shape of the Fermi surface, however, one can guess that in $CePd_2Si_2$, also in contrast to the 115 cases [two-dimensional (2D)], the correlations have mainly a 3D character. In the two cases of $CePd_2Si_2$ and $CeRh_2Si_2$,[18] the Fermi surface does not contain low-dimensional characteristics. The main difference is that in the magnetically ordered Kondo phase, the latter seems to correspond to $LaRh_2Si_2$. Let us point out that in $CeRh_2Si_2$, the pressure-induced transition to a paramagnetic ground state seems to be first order at low temperature, whereas for $CePd_2Si_2$ the picture of a smooth collapse of T_N and thus of a second-order transition at its quantum critical point is well respected.[10]

One of the fundamental dHvA frequencies is found to split into two close satellites at high field. Except for very low angles near $B \| [100]$, the satellites are likely to originate from the up and down spin bands. The effective masses corresponding to these bands differ by a factor of about 2, and both seem to be field dependent. A wave-form analysis of the oscillations suggests that this spin splitting is responsible for the peculiar shape of the field dependence of the effective mass observed in the experiment. The difference of the effective masses with spin orientations is well known in band-structure calculations of ferromagnetic metals, where the majority and minority spin Fermi surfaces are also very different. Here, however, the dHvA frequencies corresponding to different spin orientations are very close to each other, implying quite similar Fermi surfaces. The theoretical prediction that the effective mass is large and spin dependent in an almost localized Fermi liquid close to the metamagnetic transition[40] seems more plausible.

*Email address: sheikin@grenoble.cnrs.fr

[1] N.H. van Dijk, B. Fåk, T. Charvolin, P. Lejay, and J.M. Mignot, Phys. Rev. B **61**, 8922 (2000).

[2] S.K. Dhar and E.V. Sampathkumaran, Phys. Lett. A **121**, 454 (1987).

[3] I. Sheikin, Y. Wang, F. Bouquet, P. Lejay, and A. Junod, J. Phys.: Condens. Matter **14**, L543 (2002).

[4] C.D. Bredl, F. Steglich, and K.D. Schotte, Z. Phys. B **29**, 327 (1978).

[5] R.A. Elenbaas, C.J. Schinkel, and C.J.M. Van Deudekom, J.

Magn. Magn. Mater. **15–18**, 979 (1980); R. A. Elenbaas, Ph.D. thesis, University of Amsterdam, 1980.
[6] N.D. Mathur, F.M. Grosche, S.R. Julian, I.R. Walker, D.M. Freye, R.K.W. Haselwimmer, and G.G. Lonzarich, Nature (London) **394**, 39 (1998).
[7] S. Raymond, D. Jaccard, H. Wilhelm, and R. Cerny, Solid State Commun. **112**, 617 (1999).
[8] S. Raymond and D. Jaccard, Phys. Rev. B **61**, 8679 (2000).
[9] I. Sheikin, E. Steep, D. Braithwaite, J.-P. Brison, S. Raymond, D. Jaccard, and J. Flouquet, J. Low Temp. Phys. **122**, 591 (2001).
[10] A. Demuer, D. Jaccard, I. Sheikin, S. Raymond, B. Salce, J. Thomasson, D. Braithwaite, and J. Flouquet, J. Phys.: Condens. Matter **13**, 9335 (2001).
[11] A. Demuer, A.T. Holmes, and D. Jaccard, J. Phys.: Condens. Matter **14**, L529 (2002).
[12] P. Coleman, C. Pepin, Q. Si, and R. Ramazashvili, J. Phys.: Condens. Matter **13**, R723 (2001).
[13] Q. Si, S. Rabello, K. Ingersent, and J.L. Smith, Nature (London) **413**, 804 (2001).
[14] T. Senthil, S. Sachdev, and M. Vojta, cond-mat/0209144 (unpublished).
[15] G.G. Lonzarich, J. Magn. Magn. Mater. **76–77**, 1 (1988).
[16] K. Satoh, I. Umehara, N. Nagai, Y. Onuki, I. Sakamoto, M. Hunt, P. Meeson, P.A. Probst, and M. Springford, J. Magn. Magn. Mater. **104–107**, 1411 (1992).
[17] Y. Onuki, T. Komatsubara, P.H.P. Reinders, and M. Springford, J. Phys. Soc. Jpn. **58**, 3698 (1989).
[18] S. Araki, R. Settai, T.C. Kobayashi, H. Harima, and Y. Onuki, Phys. Rev. B **64**, 224417 (2001).
[19] F.S. Tautz, S.R. Julian, G.J. McMullan, and G.G. Lonzarich, Physica B **206–207**, 29 (1995).
[20] H. Aoki, M. Takashita, S. Uji, T. Terashima, K. Maezawa, R. Settai and Y. Onuki, Physica B **206–207**, 26 (1995).
[21] M. Yamanaka, M. Oshikawa, and I. Affleck, Phys. Rev. Lett. **79**, 1110 (1997).
[22] P. Fazekas, *Lecture Notes on Electron Correlation and Magnetism* (World Scientific, Singapore, 1999).
[23] A. Wasserman, M. Springford, and A.C. Hewson, J. Phys.: Condens. Matter **1**, 2669 (1989).
[24] J.W. Rasul, Phys. Rev. B **39**, 663 (1989).
[25] H. Abe, H. Kitazawa, H. Suzuki, G. Kido, and T. Matsumoto, Physica B **246–247**, 141 (1998).
[26] K. Heuser, J.S. Kim, E.W. Scheidt, T. Schreiner, and G.R. Stewart, Physica B **259–261**, 392 (1999).
[27] A. Semeno (private communication).
[28] S. Süllow, B. Janossy, G.L.E. van Vliet, G.J. Nieuwenhuys, A.A. Menovsky, and J.A. Mydosh, J. Phys.: Condens. Matter **8**, 729 (1996).
[29] K. Sugiyama, H. Fuke, K. Kindo, K. Shimohata, A.A. Menovsky, and J.A. Mydosh, J. Phys. Soc. Jpn. **59**, 3331 (1990).
[30] I. Sheikin, J. Hinderer, F. Bouquet, D. Jaccard, and S. Reymond (unpublished).
[31] M. Endo, N. Kimura, A. Ochiai, H. Aoki, T. Terashima, C. Terakura, S. Uji, and T. Matsumoto, Acta Physiol. Pol. B **34**, 1031 (2003).
[32] N. Harrison, D. W Hall, R.G. Goodrich, J.J. Vuillemin, and Z. Fisk, Phys. Rev. Lett. **81**, 870 (1998).
[33] R.G. Goodrich, N. Harrison, A. Teklu, D. Young, and Z. Fisk, Phys. Rev. Lett. **82**, 3669 (1999).
[34] O. Gunnarsson and B.I. Lundqvist, Phys. Rev. B **13**, 4274 (1976).
[35] A. Yanase, *Fortran Program for Space Group*, 1st ed. (in Japanese) (Shokabo, Tokyo, 1995).
[36] B.H. Grier, J.M. Lawrence, V. Murgai, and R.D. Parks, Phys. Rev. B **29**, 2664 (1984).
[37] N. Harrison, R.G. Goodrich, A. Teklu, L. Balicas, J.S. Brooks, D. Young, Z. Fisk, J.C. Cooley, and J.L. Smith, Physica B **294–295**, 234 (2001).
[38] L. Pricopi, E.G. Haanappel, S. Askénazy, N. Harrison, M. Bennett, P. Lejay, A. Demuer and G. Lapertot, Physica B **294–295**, 276 (2001).
[39] M. Takashita, H. Aoki, T. Terashima, S. Uji, K. Maezawa, R. Settai, and Y. Onuki, J. Phys. Soc. Jpn. **65**, 515 (1996).
[40] J. Spałek, P. Korbel, and W. Wójcik, Phys. Rev. B **56**, 971 (1997).
[41] Y. Haga, Y. Inada, H. Harima, K. Oikawa, M. Murakawa, H. Nakawaki, Y. Tokiwa, D. Aoki, H. Shishido, S. Ikeda, N. Watanabe, and Y. Onuki, Phys. Rev. B **63**, 060503(R) (2001).
[42] R. Settai, H. Shishido, S. Ikeda, Y. Murakawa, M. Nakashima, D. Aoki, Y. Haga, H. Harima, and Y. Onuki, J. Phys.: Condens. Matter **13**, L627 (2001).
[43] U. Alver, R.G. Goodrich, N. Harrison, D.W. Hall, E.C. Palm, T.P. Murphy, S.W. Tozer, P.G. Pagliuso, N.O. Moreno, J.L. Sarrao, and Z. Fisk, Phys. Rev. B **64**, 180402(R) (2001).
[44] H. Shishido, R. Settai, D. Aoki, S. Ikeda, H. Nakawaki, N. Nakamura, T. Iizuka, Y. Inada, K. Sugiyama, T. Takeuchi, K. Kindo, T.C. Kobayashi, Y. Haga, H. Harima, Y. Aoki, T. Namiki, H. Sato, and Y. Onuki, J. Phys. Soc. Jpn. **71**, 162 (2002).
[45] D. Hall, E.C. Palm, T.P. Murphy, S.W. Tozer, C. Petrovic, E. Miller-Ricci, L. Peabody, C.Q.H. Li, U. Alver, R.G. Goodrich, J.L. Sarrao, P.G. Pagliuso, J.M. Wills, and Z. Fisk, Phys. Rev. B **64**, 064506 (2001).